Optics Letters

Holographic femtosecond laser integration of microtube arrays inside a hollow needle as a lab-in-a-needle device

Shengyun Ji,[1] Rui Li,[1] Ze Cai,[1] Deng Pan,[1] Liang Yang,[1] Yanlei Hu,[1] Jiawen Li,[1,2] Dong Wu,[1,3] and Jiaru Chu[1]

[1]China Key Laboratory of Precision Scientific Instrumentation of Anhui Higher Education Institutes and CAS Key Laboratory of Mechanical Behavior and Design of Materials, Department of Precision Machinery and Precision Instrumentation, University of Science and Technology of China, Hefei 230026, China
[2]e-mail: jwl@ustc.edu.cn
[3]e-mail: dongwu@ustc.edu.cn

Received 26 July 2019; accepted 13 September 2019; posted 19 September 2019 (Doc. ID 373952); published 15 October 2019

In this Letter, the femtosecond laser holographic two-photon polymerization (HTPP) method is adopted to rapidly realize a unique lab-in-a-needle (LIN) device by manufacturing microtube arrays inside a needle. The HTPP method is to modulate a Gaussian beam into a ring Bessel beam by a spatial light modulator (SLM) loaded with a Bessel hologram, and can fabricate microtube arrays with controllable inside diameter (1–10 μm) and designable patterns on such complex three-dimensional (3D) substrates by optimizing experimental parameters. A single LIN device can be processed by this method in about 4 min, which is not possible with traditional micronano technology and is much faster than the traditional two-photon polymerization method (at least several hours). To further demonstrate the functionality of this LIN device, a particle separation experiment is carried out. For the purpose of achieving greater functionality and integration of the on-chip system, this HTPP method provides a powerful processing method for integrating 3D functional microstructures on 3D nonplanar substrates.

https://doi.org/10.1364/OL.44.005073

In recent years, To meet the ever-increasing functional requirements in different fields such as integrated optical detection and single-cell research, many new types of conceptual on-chip devices with unique advantages have been proposed [1–3]. For example, lab-in-a-tube systems have been proposed and studied in the spirit of developing increased functionality in more compact lab-on-chip (LOC) systems [1,2]. Such an ultracompact lab-in-a-tube device, which is realized by integrating multiple functional components into a single tube by rolled-up technology [4], would be independently capable of stimulating and monitoring individual cells. In addition, Koji *et al.* fabricated the 3D ship-in-a-bottle biochip by integrating various 3D polymer microstructures into flexible 3D glass microfluidic channels, which shows high performance in reagent mixing [3]. In general, these new kinds of conceptual on-chip devices have numerous unique advantages. However, the study for these devices is still in the development stage, and there are many difficulties in engineering implementation. For example, it is almost impossible to integrate high-precision functional 3D microstructures inside a tube, bottle, or needle by conventional processing techniques such as etching [5], photolithography [6], nanoimprint lithography [7], or soft lithography [8].

Femtosecond laser two-photon polymerization processing technology provides a flexible method for fabricating arbitrary shapes of 3D micro/nanostructures with its high resolution and true 3D processing characteristics [9–11]. To improve the processing efficiency of traditional single-point scanning processing method, a series of methods including microlens array [12], multibeam interference [13], diffractive optical elements [14], and spatial light modulation [15] have been proposed. In particular, the spatial light modulation technology can flexibly modulate the light field into various 3D light fields including multifocus spots [16,17], vortex beam [18], Bessel beam [19,20], and Airy beam [21] by a SLM loaded with various holograms to achieve rapid processing. However, these processing cases are currently concentrated on 2D substrates, and there are few cases on 3D substrates such as hollow needles.

In this work, we solve the difficulties of processing high-precision 3D microstructures inside the needle by a self-made clamping device combined with the femtosecond laser HTPP method for the first time. A microtube array inside the needle as a simple integrated LIN unit is rapidly processed (in about 4 min) by the femtosecond laser HTPP method. Through parametric design and optimization, microfilters with different patterns are processed. As a demonstration of filtration performance, we separate four kinds of SiO_2 microsphere mixtures with different diameters using this LIN device. To alleviate the clogging problem of the device, we adopt a blow-and-suction cycle filtration method, which greatly increases the filtration flux and proves the reusability of the device.

We previously presented the HTPP fabrication protocol for rapid processing dimension-controlled microtube arrays [22,23]. In the case of a modulating femtosecond laser Bessel beam with a reflection type liquid crystal spatial light modulator (SLM, Pluto NIR II, Holoeye, 1920 × 1080 pixels) and focusing it by a 60× oil-immersion objective, any patterns of microtube arrays with controllable inlet diameter (1–10 μm, determined by the topological charge n and the radius r_0 of the Bessel hologram [22]) and length (<150 μm, the working distance of the objective lens) can be quickly and flexibly processed inside the polymer SZ2080 [24] sample. However, HTPP processing inside a needle is more challenging than fabricating microstructures on flat substrates or even conventional 3D substrates such as grooves and curved surfaces. First of all, one of the difficulties to overcome is the clamping of the needle. How to keep the needle vertically and closely adhered to the glass substrate is the first step to achieve processing. We first put the needle in a home-made support tube and press the needle and support tube onto a cover glass by hand so that the tip of the needle stays in the same plane as the end of the support tube. Next, 50 μL of SZ2080 photoresist was dropped on the cover glass and placed on a hot plate. A small amount of photoresist was sucked into the needle. Then, as shown in Fig. 1(a), the needle is placed in the center of the cover slip and a certain force is maintained at the upper end of the needle to make the needle and the slide close together. Finally, after baking for 2 h on the 100°C hot plate [longer than the time of baking the sample on surface, Fig. 2(g)], a photoresist-containing needle adhered to the glass substrate was obtained.

To verify whether the samples are successfully prepared, the first step is to check whether there are bubbles in the photoresist inside the needle, and next is to confirm that the distance between the upper end of the needle and the glass substrate does not exceed the working distance of the objective. Only when the qualified sample is successfully prepared in the previous step, the light field can be successfully focused inside the vertical needle. Arbitrarily patterned microtube arrays can be processed inside the qualified sample by combining the focused light field and the movement of the 3D piezoelectric stage.

The HTPP processed sample is developed in the developer for about 2 days [longer than the time of developing the sample on surface, Fig. 2(h)] to obtain a microfilter integrated in the needle. The development time depends mainly on the diameter and length of the microtube. The smaller the microtube diameter and the longer the length is, the longer the development time will be. To balance the stability of the structure and the development time, a compromised length (~40 μm) is chosen here. Such an integrated filtration device can be conveniently used for high-throughput particle filtration or rare particle enrichment. Moreover, to further increase the filtration flux, a manual blow-and-suction cycle method [Fig. 1(d)] can be used for multiple cycle filtration.

In the case of HTPP processing of microtube arrays, the processing time of each microtube with a length of ~40 μm is about 1 s regardless of the diameter of the microtube. For example, in this work, microtubes with an average diameter of 10 μm and a height of 40 μm are processed inside a needle with an inner diameter of 160 μm. When the platform scans progressively, the scanning path is reasonably optimized according to the diameter of the needle and microtube, so that the processing is performed only in the circular area of the needle. Thus, the number of microtubes can be reduced to 250, and the total processing time is only ~4 min, which is much shorter than the time of single-point scanning [~8 h, scanning interval: 200 nm, single point's exposure time: 1 ms, Fig. 2(i)].

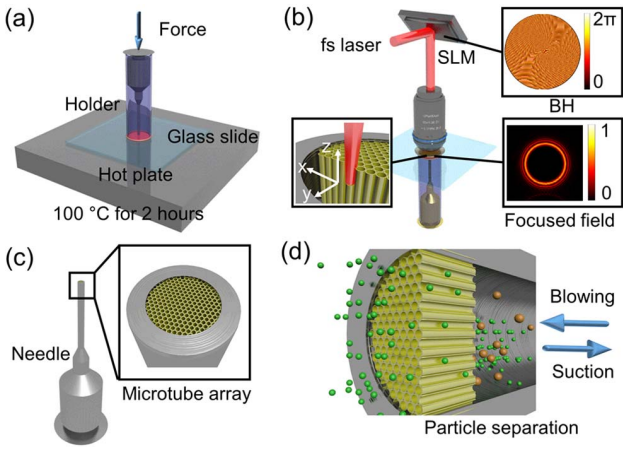

Fig. 1. Schematic illustration of rapid processing microtube arrays in a needle by HTPP processing and the filtration process. (a) The needle placed in a home-made holder is pressed by a certain force onto the glass slide with photoresist and baked for 2 h at 100°C. (b) The phase-modulated ring light field is focused by an objective into the needle for rapid microtube array processing. The inserts are the HTPP process (left), Bessel hologram (BH, top right) loaded on the SLM and the simulated focused field (bottom right). (c) Schematic diagram of the microtube array inside the needle after the photoresist is developed. (d) A blow-and-suction method is adopted to reduce the clogging problem and improve separation flux.

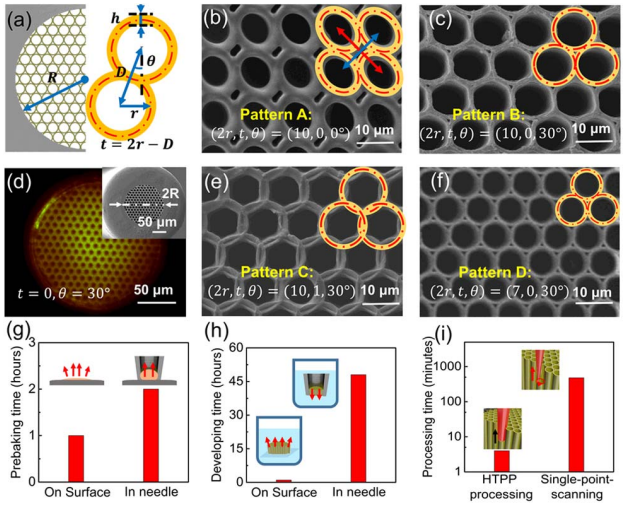

Fig. 2. Schematic diagram of the layout of different microtube arrays in the needle and the quantitative processing parameters. (a) The microtube array is processed inside the needle with inner diameter R as the filter. Three parameters ($2r$, t, θ) are mainly designed. (b), (c), (e), (f) Different patterns have been fabricated. (d) The fluorescence microscopic image of the microtube array with the same parameters as (c) inside the needle. The insert is the SEM image. Differences of (g) the prebaking time and (h) developing time between samples on the surface and samples inside the needle. (i) The total processing time by HTPP processing and single-point scanning.

When processing microtubes inside a needle with an inner radius of R, three parameters are mainly considered in the pattern design. As shown in Fig. 2(a), one is the average radius of the microtube, defined as r. One is the interval between two adjacent microtubes, defined as t. The center distance of two adjacent microtubes with wall thickness h is D, and t can be given by the following formula:

$$t = 2r - D. \tag{1}$$

The last one is the angle between the adjacent microtubes in different columns, defined as θ. Different patterns with different $(2r, t, \theta)$ combinations have been fabricated [Figs. 2(b), 2(c), 2(e), 2(f)], including (10 μm, 0, 0°), (10 μm, 0, 30°), (10 μm, 1 μm, 30°), (7 μm, 0, 30°).

To study the effect of different parameter combinations on the processing results of patterned microtube arrays, the following three sets of control experiments are illustrated. First, the microtube arrays with the same average diameter $2r = 10$ μm and the same interval $t = 1$ μm can be divided into square and hexagonal arrangement. Comparing the roundness and wall thickness of the microtubes in Figs. 2(b) and 2(c), it is easy to conclude that the hexagonal-arranged patterned microtube array structure can maintain the original design shape. The shape modulation phenomenon in Fig. 2(b) is mainly caused by the existence of internal stress and the structural instability of the square arrangement. Second, when the microtube arrays are with the same diameter of $2r = 10$ μm and the same angle of $\theta = 30°$, the intersection of the HTPP region due to the difference of t will cause a significant change in the internal shape of the tube [Figs. 2(c) and 2(e)]. When the interval between two adjacent microtubes satisfies $t = 0$, both the tight connection between adjacent microtubes can be ensured, and the internal shape of the tube can be prevented from being damaged. Third, when the interval of adjacent microtubes $t = 0$ and the angle $\theta = 30°$ in the microtube array remain the same, the effect of microtube diameter difference on the structure is not so obvious.

According to the discussion in the previous section, we selected the microfilter with the parameter combination of $(2r, t, \theta)$ = (10 μm, 0, 30°) as a demonstration of the particle separation experiment. After the mixture of the particles to be sorted was sucked into a sterile disposable syringe, the integrated needle filter device was mounted on the syringe [Fig. 3(a)]. This allows for manual particle separation or automatic separation by a syringe pump.

In the separation experiment, the results of sorting four kinds of monodispersed SiO_2 microsphere [Fig. 3(d)] with different diameters (2.5, 5, 10, 20 μm) were used to demonstrate the experimental performance of the filtration device. First, each kind of particle was formulated into a mixture of mass/volume percentage concentration of 0.6 w/v% using ethanol as a solvent. Next, we conducted two types of separation experiments: Type I, separation of two kinds of particle mixtures, Type II, separation of four kinds of particle mixtures.

In the Type I experiment, 0.25 mL of each of two different diameter SiO_2 microsphere mixtures (2.5 and 20 μm in diameter) totaling 0.5 mL was taken as the mixture to be separated [Fig. 3(b)]. To achieve more efficient particle separation, a manual blow-suction cycle method was adopted to reduce the clogging problem. During the blowing process, push the syringe with the thumb until the particles block the filter.

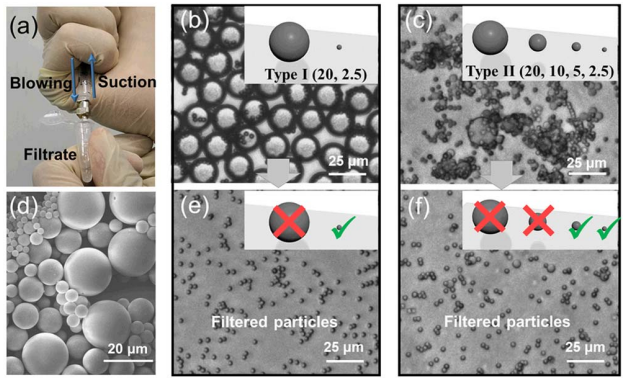

Fig. 3. Simple handheld filtration device and two types of particle sorting results. (a) Simple integrated particle separation unit. (b) and (c) are the microscopic images of different kinds (Type I and Type II) of particle mixture. The insert shows different kinds of SiO_2 particles with different diameters. (d) SEM image of four kinds of SiO_2 particles. (e) and (f) are the microscopic images of filtered particles.

To prevent droplet leakage and even structural damage, the pressure is kept within ~30 psi. At a high particle concentration of ~10^8 particles/mL, single filtration could only obtain a maximum of 0.05 mL of filtrate. However, after 16 cycles of filtration in about 3 min, about 60% of the mixture was filtered into a microcentrifuge tube. Multiple cycles of filtration could greatly increase the filtration flux of the unit. Whether it is single filtration or multiple filtration, the filtrate obtained contains only one microsphere of 2.5 μm diameter [Fig. 3(e)]. To further test the ability of the device to separate a variety of particles, a total volume of 0.5 mL of four equal amounts of different diameters microsphere mixtures was used in Type II separation experiment [Fig. 3(c)]. The same method was used to sort four different diameters microspheres.

To quantitatively evaluate the performance of the LIN device, the geometric characteristics of the microtubes in four different patterned microfilters (Patterns A–D), including the aspect ratio (AR) and the average inner diameter (AD) distribution, were analyzed quantitatively. First, as shown in Fig. 4(a), from the aspect ratio of the microtube, except for Pattern A, the aspect ratio in other patterned microfilters is within 1.1, which fully demonstrates that the hexagonal arrangement is more conducive to the stability of the overall structure than the square arrangement. At the same time, compared with Patterns B and D, the smaller the diameter of the microtube, the closer the aspect ratio is to 1, which means that reducing the microtube diameter to a certain extent is more conducive to structural stability. Second, from the inlet diameter of the microtube [Fig. 4(b)], the box and whisker plots show that only the average inlet diameters of Patterns B and D are almost the same as the designed inlet diameter. Combining the data of the aspect ratio, the parameter combination of $(t, \theta) = (0, 30°)$ is more suitable for designing a stable and reliable microfilter.

For the particle separation experiment, we first quantitatively analyzed the multiple filter-rinse cycle experimental data to verify the stability of the device. Taking Type I of two particle separation as an example, after single filtering 0.5 mL particle mixtures of two different diameter microspheres, the deionized water was sucked into the syringe

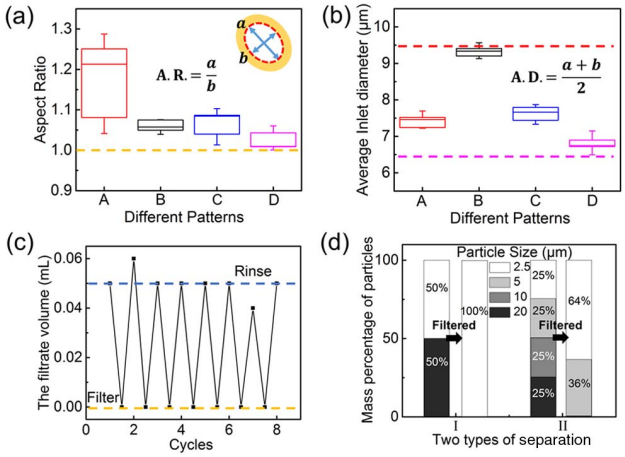

Fig. 4. Quantitative data statistics for dimensional characteristics of microtubule arrays with different patterns and SiO_2 particles separation. The box and whisker plots show (a) the aspect ratio and (b) the average inlet diameter distribution (red line: designed inlet diameter 9.5 μm for Patterns A, B, and C, magenta line: designed inlet diameter 6.5 μm for Pattern D) of the microtubes with different patterns of 15 μm in thickness. The boxes contain percentiles 25 to 75, and the whiskers correspond to the maximum and minimum values. (c) The line chart shows the volume of the filtrate obtained per cycle (0.05 ± 0.01 mL). (d) The bar chart shows the volume percentage of four kinds of SiO_2 particles before and after Types I and II separation.

through the needle microfilter to clean up the blocked particles. Next, the rinsed microfilter was mounted on the syringe that had the same volume of the mixture inhaled and performed a new filtration. Fig. 4(c) illustrates that the volume of the filtrate obtained per cycle was substantially the same (0.05 ± 0.01 mL). The stability of the device is guaranteed by the hexagonal arrangement and the height of the microtube.

The mass percentages of the different particles in the filtrate after the two types of filtration are shown in Fig. 4(d). From the results of several experiments, it was found that only one kind of microsphere with the diameter of 2.5 μm was found in the filtrate after Type I single filtration. As for the Type II filtration experiment, it is notable that the ratio of the number of 2.5 μm diameter microspheres to the 5 μm microspheres in the filtrate is larger than the proportion of the two particles in the original mixture. We suspect that small particles are easier to pass through the microfilter because the flow resistance produced by small particles flowing through the microtubes is smaller than when the large particles pass through the microtubes.

In this study, the femtosecond laser HTPP processing method was adopted to flexibly integrate microtube arrays inside a commercial stainless-steel needle as a LIN concept device. Technically, we have solved two crucial difficulties in engineering implementation: (1) The difficulty of processing high-precision 3D microstructures inside a needle is solved by the photoresist sample preparation with a self-made clamping device combined with high-precision HTPP processing technology. (2) The stability and consistency of the microstructures integrated inside the needle, which is the basic guarantee for the specific function of the device, are ensured by the flexible processing characteristics of the HTPP processing method through processing parameter optimization and pattern design. In two types of separation experiment, the filtering results of the mixture of different kinds of monodispersed SiO_2 microsphere with high particle concentration were used to verify the performance of the filter device. A single filtration of 0.5 mL SiO_2 microsphere mixture with diameters of 2.5 and 20 μm yields 0.05 mL of monodisperse filtrate containing only 2.5 μm diameter particles.

Funding. Key Project of Equipment Pre-research Field Fund of China (61409230310); National Natural Science Foundation of China (51675503, 51875544, 61475149, 61805230); National Key R&D Program of China (2018YFB1105400).

REFERENCES

1. J. Smith, S. Schulze, S. Kiravittaya, Y. Mei, S. Sanchez, and O. G. Schmidt, Nano Lett. **11**, 4037 (2011).
2. J. Smith, W. Xi, D. Makarov, I. Monch, S. Harazim, V. A. Bolanos Quinones, C. K. Schmidt, Y. Mei, S. Sanchez, and O. G. Schmidt, Lab Chip **12**, 1917 (2012).
3. D. Wu, S. Z. Wu, J. Xu, L. G. Niu, K. Midorikawa, and K. Sugioka, Laser Photon. Rev. **8**, 458 (2014).
4. G. Schmidt and K. Eberl, Nature **410**, 168 (2001).
5. F. Chen, C. Shan, K. Liu, Q. Yang, X. Meng, S. He, J. Si, F. Yun, and X. Hou, Opt. Lett. **38**, 2911 (2013).
6. J. B. Hutchison, K. T. Haraldsson, B. T. Good, R. P. Sebra, N. Luo, K. S. Anseth, and C. N. Bowman, Lab Chip **4**, 658 (2004).
7. J. Chen, Y. Zhou, D. Wang, F. He, V. M. Rotello, K. R. Carter, J. J. Watkins, and S. R. Nugen, Lab Chip **15**, 3086 (2015).
8. S. N. Bhatia and D. E. Ingber, Nat. Biotechnol. **32**, 760 (2014).
9. S. Kawata, H. B. Sun, T. Tanaka, and K. Takada, Nature **412**, 697 (2001).
10. M. Malinauskas, A. Žukauskas, S. Hasegawa, Y. Hayasaki, V. Mizeikis, R. Buividas, and S. Juodkazis, Light Sci. Appl. **5**, e16133 (2016).
11. M. Farsari and B. N. Chichkov, Nat. Photonics **3**, 450 (2009).
12. J. I. Kato, N. Takeyasu, Y. Adachi, H. B. Sun, and S. Kawata, Appl. Phys. Lett. **86**, 044102 (2005).
13. T. Kondo, S. Matsuo, S. Juodkazis, V. Mizeikis, and H. Misawa, Appl. Phys. Lett. **82**, 2758 (2003).
14. Y. Kuroiwa, N. Takeshima, Y. Narita, S. Tanaka, and K. Hirao, Opt. Express **12**, 1908 (2004).
15. A. M. Weiner, Rev. Sci. Instrum. **71**, 1929 (2000).
16. K. Obata, J. Koch, U. Hinze, and B. N. Chichkov, Opt. Express **18**, 17193 (2010).
17. S. D. Gittard, A. Nguyen, K. Obata, A. Koroleva, R. J. Narayan, and B. N. Chichkov, Biomed. Opt. Express **2**, 3167 (2011).
18. S. J. Zhang, Y. Li, Z. P. Liu, J. L. Ren, Y. F. Xiao, H. Yang, and Q. Gong, Appl. Phys. Lett. **105**, 061101 (2014).
19. N. Chattrapiban, E. A. Rogers, D. Cofield, W. T. Hill III, and R. Roy, Opt. Lett. **28**, 2183 (2003).
20. L. Yang, A. El-Tamer, U. Hinze, J. Li, Y. Hu, W. Huang, J. Chu, and B. N. Chichkov, Appl. Phys. Lett. **105**, 041110 (2014).
21. G. A. Siviloglou, J. Broky, A. Dogariu, and D. N. Christodoulides, Phys. Rev. Lett. **99**, 213901 (2007).
22. S. Ji, L. Yang, Y. Hu, J. Ni, W. Du, J. Li, G. Zhao, D. Wu, and J. Chu, Small **13**, 1701190 (2017).
23. S. Ji, L. Yang, C. Zhang, Z. Cai, Y. Hu, J. Li, D. Wu, and J. Chu, Opt. Lett. **43**, 3514 (2018).
24. Ovsianikov, J. Viertl, B. Chichkov, M. Oubaha, B. MacCraith, I. Sakellari, A. Giakoumaki, D. Gray, M. Vamvakaki, M. Farsari, and C. Fotakis, ACS Nano **2**, 2257 (2008).